Acta Cryst. (1975). A31, 784

Ordering of the Point Defects in Nonstoichiometric Crystals of $Nb_{12}O_{29}$

BY SUMIO IIJIMA

Department of Physics, Arizona State University, Tempe, Arizona 85281, *U.S.A.*

(*Received* 11 *April* 1975; *accepted* 27 *May* 1975)

The reduction of crystals of $Nb_{12}O_{29}$, having an excess of oxygen, has been studied by high-resolution electron microscopy and electron diffraction. A superstructure and faulted slabs are formed, by aggregation of the point defects forming chains with a limited length in the matrix structure, induced by electron-beam irradiation. Ordering of the chains of point defects in the crystals is directly observed by electron microscopy with resolution of the atomic level. A mechanism for the dissipation of the point defects is discussed in terms of the reduction and oxidation of the nonstoichiometric crystals of $Nb_{12}O_{29}$.

Introduction

The phase $Nb_{12}O_{29}$ is the lowest niobium oxide between NbO_2 and Nb_2O_5 in the phase diagram, where many phases are known, all based on the ReO_3-type structure and structurally closely related. Similar structures are abundant in ternary Nb oxides of Ti, W and Zr. A common feature in these structures is a crystallographic shear (CS) plane, where metal–oxygen octahedra join by sharing their edges. The CS planes are arrayed two-dimensionally and divide a slab of the ReO_3 type into small blocks of $m \times n$ octahedra, where m and n are 3 to 5, depending on the composition of a crystal. In some crystals metal atoms having tetrahedral coordinations occur near the corners of the blocks. Occurrence of the CS planes in a crystal contributes to the deficiency of the oxygen.

One of the interests in these materials is the transformation which occurs in the solid state on oxidation or reduction of a crystal. Rearrangement of the CS planes results in the transformation from one structure to another. The elucidation of the diffusion mechanism for cations and anions involved in transformations has been sought for the past decade. A simple example of a CS plane has been studied in slightly reduced WO_3 crystals and the mechanism for the formation of the CS plane was discussed (Iijima, 1975*a*).

In a previous paper (Iijima, Kimura & Goto, 1973), we reported that the crystals of $Nb_{12}O_{29}$ having a slight excess of oxygen contained point-defect complexes consisting of two displaced niobium atoms and two extra oxygen atoms. Thus, occurrence of these defects contributes to the nonstoichiometry of the crystal of $Nb_{12}O_{29}$. Similar point defects were also found in nonstoichiometric crystals of $Nb_{22}O_{54}$ and the role of these point defects was discussed (Iijima, Kimura & Goto, 1974).

Visualization of point defects became possible under some circumstances by highly controlled high-resolution electron microscopy developed in our laboratory. Such experiments suggested the possibility of seeing directly the reorganization of the atoms in the crystal under the microscope.

In the present experiment, slightly oxidized crystals of $Nb_{12}O_{29}$ were examined at various stages of electron-beam irradiation by means of both electron diffraction and electron microscopy. A short-range order of the point defects, a superstructure and faulted slabs due to rearrangement of the point-defect complexes, and reorganization of CS planes were observed. The nature of the point defects which we have not previously described is considered and a mechanism for the dissipation of the point defects is discussed in terms of reduction and oxidation.

Experimental

The samples of slightly oxidized $Nb_{12}O_{29}$ (black color) have a composition of $NbO_{2.418}$. The stoichiometric composition is $NbO_{2.4166}$. They were prepared by oxidizing NbO_2 at 1400°C in a CO_2/H_2 gas mixture and the detailed procedure for the preparation has been reported by Kimura (1973). Fragments from the samples ground in an agate mortar were collected on holey carbon supporting films. Very thin crystallites were chosen and aligned with a goniometer stage to orient the b axis parallel to the incident electron beam. The necessary imaging conditions have been discussed previously (Iijima, 1973).

For studying the effects of the electron-beam irradiation on the crystals, the intensity of the beam and the exposure time were varied.

Observation and interpretation

Point defects

In the previous study (Iijima, Kimura & Goto, 1973) on the crystals of $Nb_{12}O_{29}$ having an excess of oxygen, it was found that these crystals were reduced under weak electron-beam irradiation and the point-defect complexes disappeared, resulting from release of oxygen atoms from the crystals, and the crystals became stoichiometric. The phase equilibrium study on niobium oxides suggests that $Nb_{12}O_{29}$ is very easily oxidized and may not be reduced even in the ordinary vacuum of the microscope (10^{-5} Torr). Then we

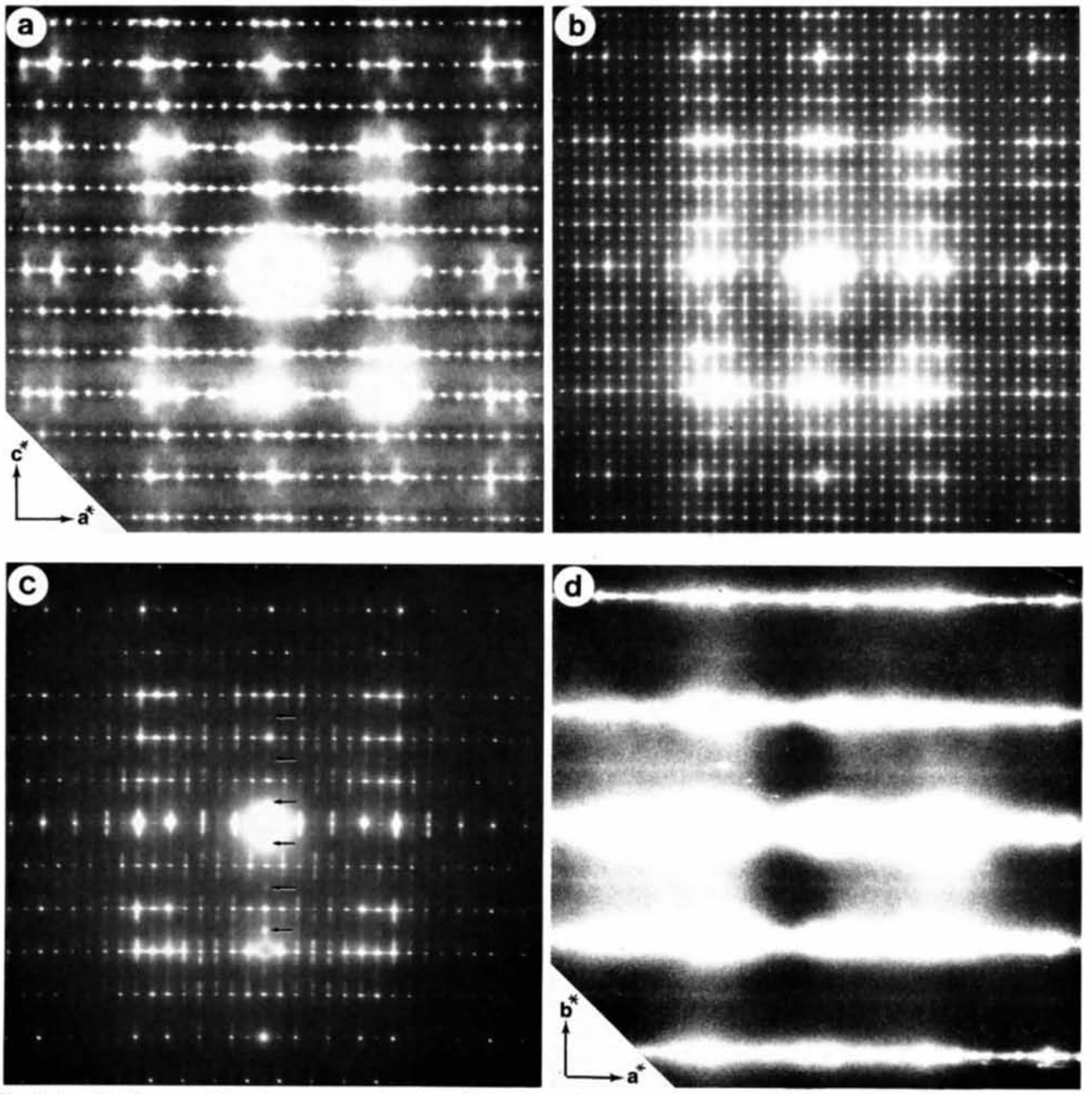

Fig. 2. (*a*)–(*c*) Electron diffraction patterns showing a^*c^* reciprocal sections. (*a*) From the original crystal of $Nb_{12}O_{29}$ having a slight excess of oxygen, showing diffuse scattering. (*b*) After intense electron-beam irradiation, showing superstructure spots. (*c*) With further electron-beam irradiation, showing streaks along [001]. Note that the (0, 0, $2n+1$) reflections (arrowed) that are forbidden for the host lattice of ortho-$Nb_{12}O_{29}$ appear. (*d*) An a^*b^* reciprocal section of the original crystal of $Nb_{12}O_{29}$, showing diffuse streaks.

[*To face p.* 784

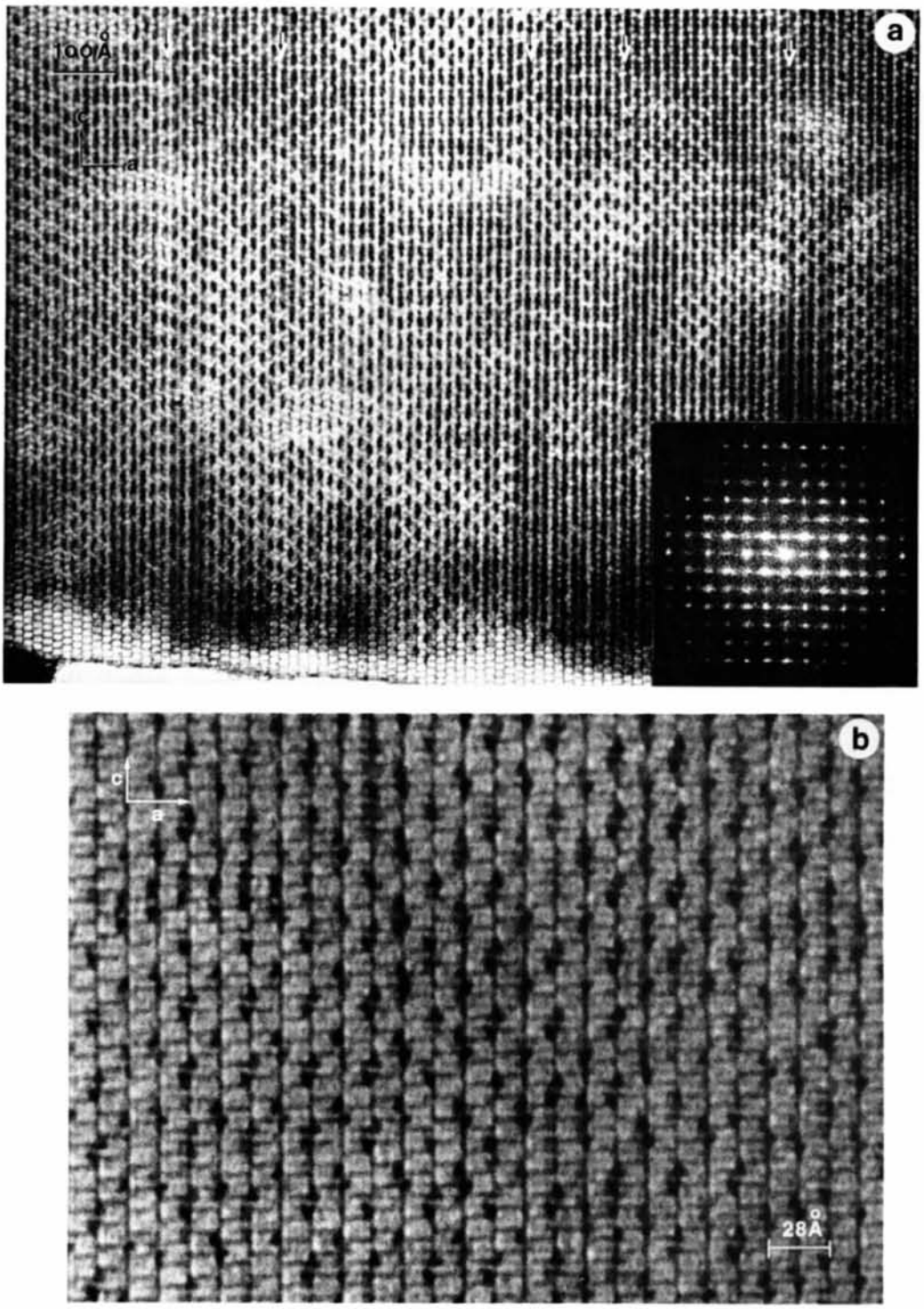

Fig. 3. (*a*) A two-dimensional lattice image of the crystal giving superstructure spots [see Fig. 2(*b*)]. The inset is the optical diffraction pattern taken from the image. Arrows indicate the positions of stacking faults occurring on (100) planes where the regular arrays of the black spots are disturbed. (*b*) A high-resolution lattice image showing the superstructure where paired black spots are regularly arrayed in the matrix structure of ortho-$Nb_{12}O_{29}$.

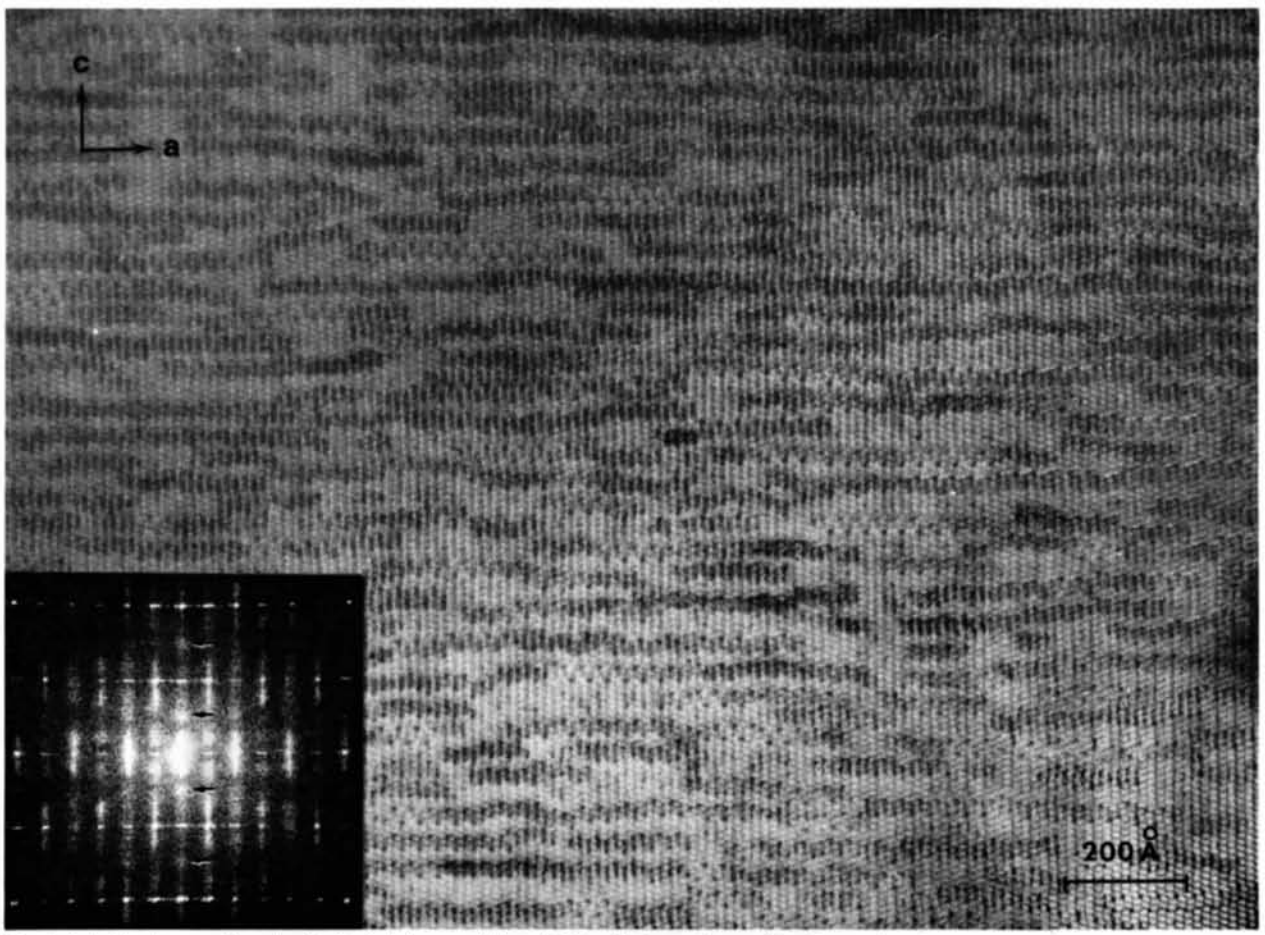

Fig. 6. A lattice image showing faulted slabs parallel to [100] which are formed by destroying the superstructure due to the further electron-beam irradiation. The inset is the optical diffraction pattern taken from the image. The forbidden spots (arrows), similar to those in the electron diffraction pattern [Fig. 2(*c*)], result from the faulted slabs.

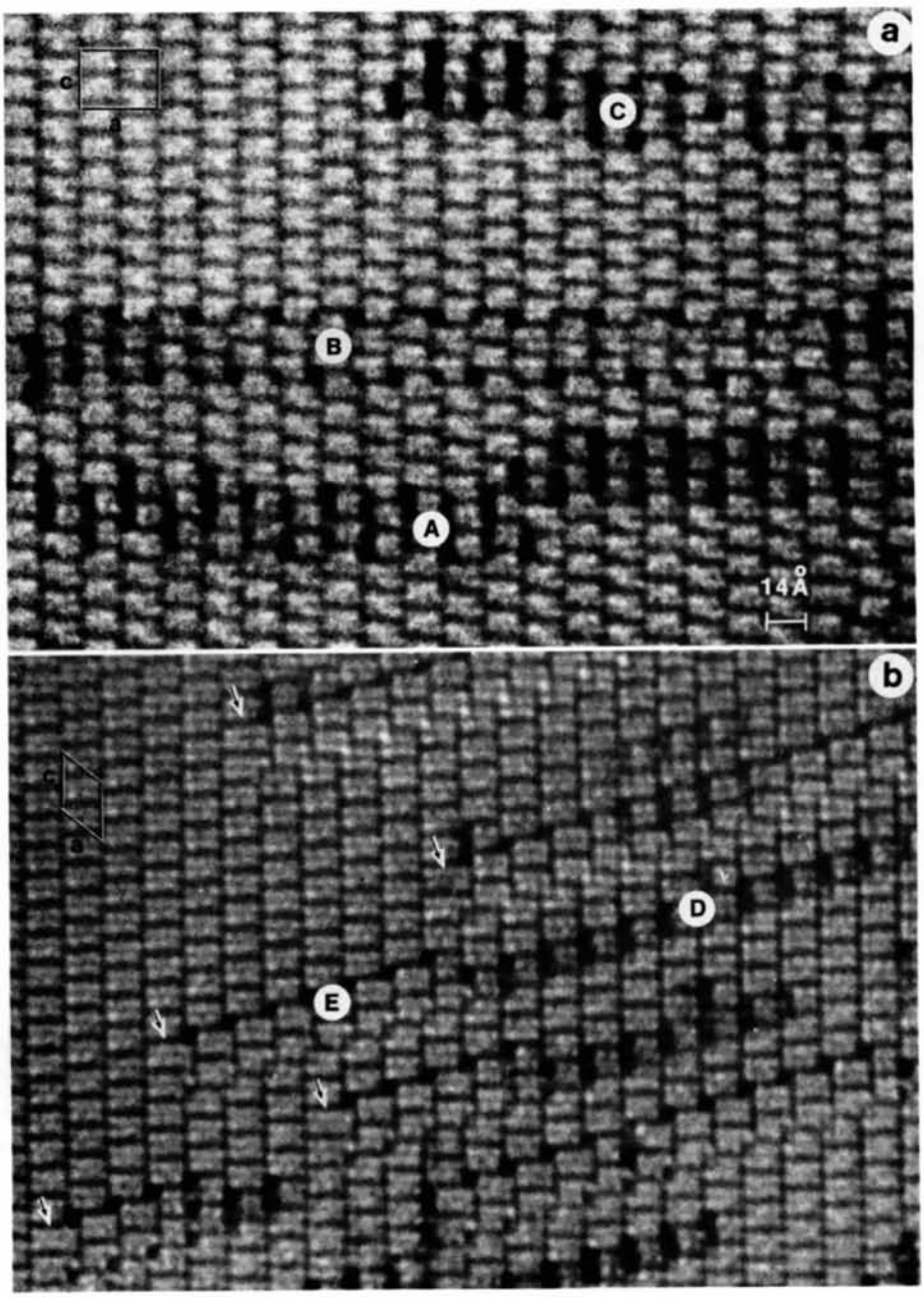

Fig. 7. (*a*) The faulted slabs occurring in the crystal of ortho-$Nb_{12}O_{29}$, showing two types of contrast, (*A* and *B*) and their mixture (*C*). Note the displacements of the 3×4 blocks in the slab *B*. (*b*) Similar faulted slabs (*E* and *D*) but occurring in mono-$Nb_{12}O_{29}$. Note the creation of the 3×5 blocks (arrowed).

thought that the reduction of the crystals may be enhanced owing to temperature increase of the specimen as well as energy transfer from the electron beam to the crystal. Some catalytic reactions involving carbon could allow the removal of the oxygen from the crystal surface. However, the true mechanism for the reduction has not been clearly understood.

Fig. 1 reproduces our previously proposed model for the point-defect complexes (Iijima, Kimura & Goto, 1973). The defect consists of two Nb atoms displaced from the normal sites of the matrix and two extra oxygen atoms. One of the displaced Nb atoms (indicated by *a*) is tetrahedrally coordinated. The defects are formed at crystallographically equivalent sites in the unit cell (marked ×) and we suspected that presumably they are randomly distributed at those sites through the crystals. The area of the defect (shaded in Fig. 1) appeared as black spots in the electron micrograph but we did not know how many defects are superimposed on top of one another along the incident electron beam direction parallel to [010] to generate a black contrast.

With a strong electron-beam irradiation the crystals were changed in a quite different way from that observed previously with relatively weak beam irradiation. This difference may be caused by a different diffusion process of the oxygen atoms in the crystals which may be affected by the intensity of the electron beam. The crystals showed two typical stages before being completely reduced.

Fig. 2(*a*) is an electron diffraction pattern taken from the original crystal of ortho-$Nb_{12}O_{29}$ containing the point defects. It shows very weak diffuse scattering between the lines of spots parallel to **a*** which we failed to observe previously probably because they are very weak. This diffuse scattering apparently results from the point defects. On the other hand, an a^*b^* reciprocal lattice plane section from the original crystal [Fig. 2(*d*)] also shows weak continuous diffused lines halfway between $0k0$ spots. This indicates that, although we thought previously that the point defects were randomly distributed, they actually tend to be aligned along [010] with a periodicity of $2b$, forming chains of the defects. The fluctuation in the contrast of the defects that was reported previously (see Fig. 3 of Iijima, Kimura & Goto, 1973) can be explained by the limited length of the chains of the point-defect complexes along [010]. This will be discussed later.

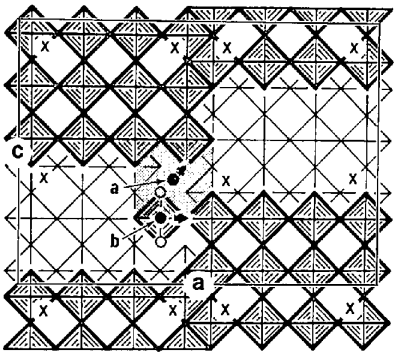

Fig. 1. A model for the point-defect complex composed of two interstitial metal atoms [at a tetrahedral position (*a*) and at an octahedral position (*b*)] and two oxygen atoms (open circles). The shaded area forms a column of a chain of tetrahedral positions extending along [010]. ×'s represent possible sites for the point defect. The unit-cell of the ortho-$Nb_{12}O_{29}$ structure is outlined.

Superstructure

When the crystals are irradiated with an intense electron beam for several seconds, the diffuse scattering that was observed in the original crystals disappears and superstructure spots appear [Fig. 2(*b*)]. This transformation is accomplished almost instantly but the intensities of the superstructure spots decrease with further exposure of the crystal to the intense beam.

The superstructure has a unit cell with $a_s=a$, $c_s=3c$ (for ortho-$Nb_{12}O_{29}$, $a=28{\cdot}90$, $b=3{\cdot}835$, $c=20{\cdot}72$ Å). Similar superstructure diffraction spots were observed in crystals of ortho-$Nb_{12}O_{29}$ oxidized in a controlled atmosphere by Browne, Hutchison & Anderson (1972). They described the superstructure as the 'Ox-II' phase obtained by oxidation of ortho-$Nb_{12}O_{29}$ at 650°C. This was first found by Schäfer (1966) but the crystal structure was not determined.

The electron micrograph corresponding to the electron diffraction pattern of Fig. 2(*b*) shows black spots arrayed periodically in some areas, forming domains, but a random distribution of the black spots in other areas [Fig. 3(*a*)]. The image of the latter regions is similar to that observed in the original crystal [see Fig. 6(*a*)] of Iijima, Kimura & Goto, 1973], suggesting that those areas are unchanged. The inset of Fig. 3(*a*) is an optical diffraction pattern from the image of Fig. 3(*a*), which corresponds well to Fig. 2(*b*).

Another finding is that the regularity of the arrays of the black spots is interrupted by stacking faults (indicated by arrows) which are caused by accidental occurrences of the monoclinic form of $Nb_{12}O_{29}$, one or two unit cells wide. The superstructure was formed only in thicker regions (more than 300 Å thick) of larger crystals (roughly greater than 5 μm diameter). This dependence on the crystal thickness and size seems to be due to the difference in the specimen temperature during the electron-beam irradiation or access to crystal surface.

Fig. 3(*b*) is a high-magnification image of a region of the superstructure. It is seen that pairs of black spots that appeared as single black spots in Fig. 3(*a*), are formed in two 3×4 blocks, which are diagonally neighboring across the CS planes (continuous dark lines along [001] in the image) and they repeat every three blocks along [001]. The contrast of each black spot is similar to that of the linear chain of the point defects even though these images were recorded from a thicker region of the crystal (estimated crystal thickness

is about 300 to 500 Å).* From the similarity, the structure causing a pair of black spots may be described by using our previously proposed model for the point defect complex (Fig. 1). A temporary model for the defect structure is illustrated in Fig. 4(*a*) and its simple representation in Fig. 4(*b*). This will be discussed later. The locations of the defect pairs obtained from Fig. 3(*b*) are schematically illustrated in Fig. 5 (indicated by squares). The superstructure has a unit cell of $a_s = a$, $c_s = 3c$ (outlined by dotted lines), in accordance with the observation of the superstructure diffraction spots of Fig. 2(*b*). The unit cell is orthorhombic or monoclinic. In the latter case the c_s is inclined from the plane of the paper and α will be arctan $2b/3c$ and the unit cell becomes one half of the orthorhombic cell. Note the 3×4 blocks drawn by light lines in Fig. 5 are located by $\frac{1}{2}b$ below the plane of the page. We failed to observe an *ab* section of crystals containing the superstructure, but according to Browne, Hutchison & Anderson (1972) the b_s axis of the 'Ox-I' phase, having a structure related to mono-$Nb_{12}O_{29}$ is doubled.

For this model four extra oxygen atoms are necessary for each pair of defects with respect to the stoichiometric structure. If the model [Fig. 4(*a*)] is correct, the metal–oxygen ratio in a region of the superstructure turns out to be 2·528. Apparently this is unlikely because the highest known Nb oxide is Nb_2O_5, *i.e.*, O/M = 2·500. If, as we mentioned before, the b_s axis is doubled, the ratio becomes 2·472. If we considered that the superstructure is a transitional state of the transformation to Nb_2O_5 as suspected by Schäfer *et al.* (1966), the figure seems to be reasonable.

From the observation of the superstructure we may draw one obvious conclusion that the superstructure was formed by the aggregation of the linear chains of the point-defect complexes. Note that if the two extra oxygen atoms (open circles in Fig. 1) are released from a point-defect complex and then the displaced metal atoms (solid circles in Fig. 1) go back to their normal sites in the matrix structure, the defect is completely removed. The released oxygen atoms migrate through the crystal and will make a new defect at a different location unless they migrate to the crystal surface and escape from the crystal. In this way the linear chains of point defects can apparently move around.

If we look at only the region of the superstructure, we may say that the original crystal (O/M = 2·418) has actually been oxidized instead of reduced. Because of a limited environment in the microscope, the superstructure seems to grow only as domains, as seen in Fig. 3(*a*).

* We found previously that lattice images of the 'block structures' showing metal atom positions in the structures reappear at a thicker region of crystals as well as at a very thin region (less than 100 Å) (Fejes, Iijima & Cowley, 1973). In the present report all images were recorded from thick crystals. Theoretical evaluations of such images have not been done but experimentally there seems to be no essential difference between these two types of image except for a slight loss of resolution.

Faulted slabs

With further electron-beam irradiation the superstructure is destroyed and planar defects of limited width are formed which are parallel to (001) and appear as dark bands running parallel to [100] (Fig. 6). This change is rather slow and these faults form first in a thin region of the crystal and then progress toward a thicker region. The electron diffraction pattern from the same crystal giving the electron micrograph of Fig. 6 shows strong diffuse streaks developed parallel to [001] at the fundamental reflections [Fig. 2(*c*)]. The streaks have broad maxima at the positions of $\frac{1}{4}$ to $\frac{1}{3}$ of d_{002}, and this fraction decreases with the time of the exposure, implying that the average distance between the slabs along [001] is 30 to 40 Å. The optical diffraction pattern (the inset of Fig. 6) from the negative of the electron micrograph of Fig. 6 shows a similar pattern to Fig. 3(*c*), so that the diffuse streaks are definitely

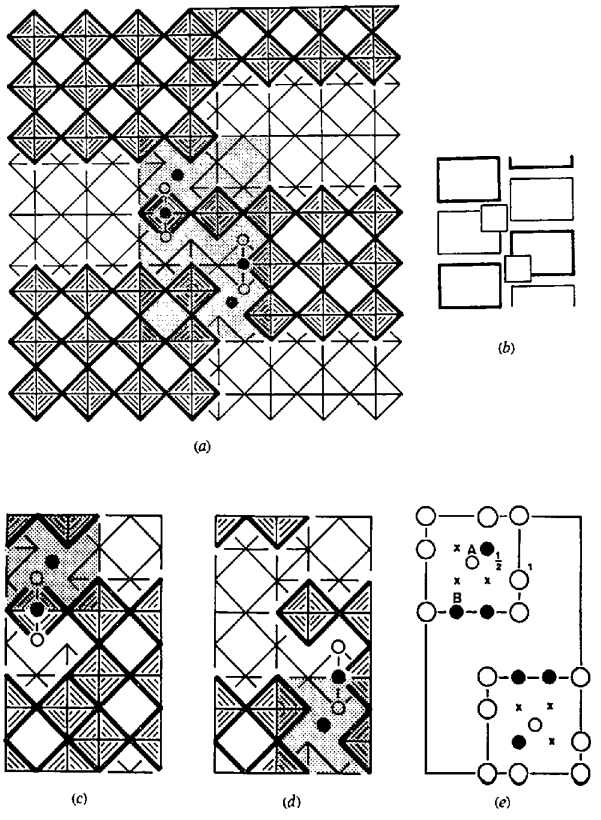

Fig. 4. (*a*) A temporary model for the defect giving a pair of the black spots of Fig. 3(*b*) consisting of two point-defect complexes of Fig. 1 that form linear chains along [010]. (*b*) Its simple representation. A proposed model for the paired chains of the point defect complexes is slightly modified from the one in (*a*) and is a superposition of the two structures shown in (*c*) and (*d*) [only shaded area of (*a*) is shown]. They are alternately stacked along [010]. (*e*) An *ac* plane projection of the defect pairs, showing apparent occupancies of the metal atoms in the tetrahedral column. Atoms A and B can also go to the positions indicated by the ×'s.

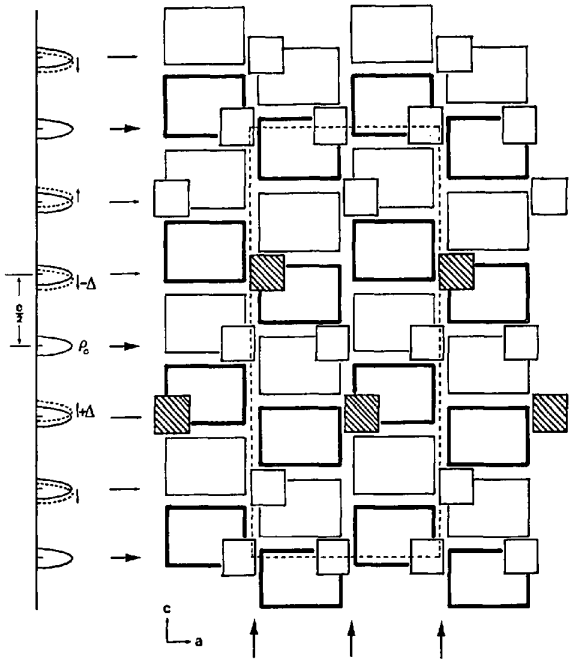

Fig. 5. A model showing a distribution of the linear chains of point defects in the matrix structure which is derived from the Fig. 3(*b*). The unit-cell of the superstructure is outlined with dotted lines.

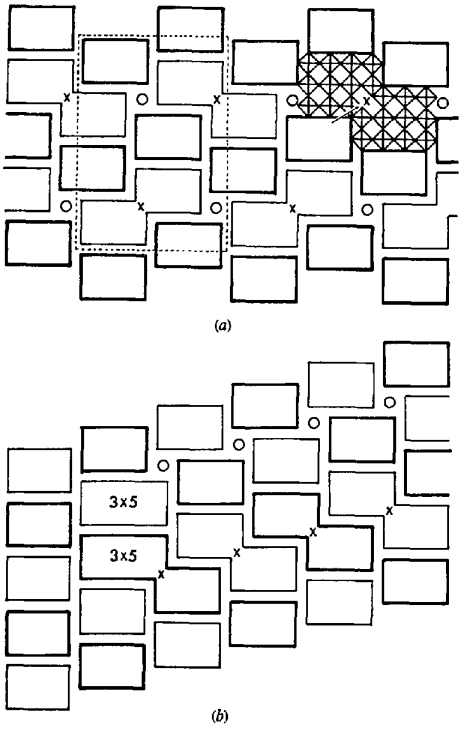

Fig. 8. A possible model for the faulted slab *B* in Fig. 7(*a*) where the tetrahedral positions (see Fig. 1), displacements of the 3×4 blocks and irregular joining of the blocks (shown by $\times$'s) occur. (*b*) A model for the faulted slab *E* in Fig. 8(*b*). At the termination of the slab the 3×5 blocks are formed.

due to the faulted slabs. Note that the $(0,0,2n+1)$ reflections [arrowed in Fig. 2(*c*)], which are forbidden for a space group *Amma* of the crystal ortho-$Nb_{12}O_{29}$, appear and they are also observed in the optical diffraction pattern (arrowed).

Two types of contrast in the faulted slabs were commonly observed [marked *A* and *B* in Fig. 7(*a*)]. The defect marked *A* appears to be an aggregation of the linear chains of point defects into a slab roughly parallel to (001). The other, marked *B*, contains periodic arrays of black spots and within a slab the 3×4 blocks are displaced from the normal positions. A possible model for the defect slab *B* is illustrated in Fig. 8(*a*). The periodicity of *a* in the matrix along [100] is retained in the slab but the width of the slabs is $\frac{3}{2}c$, where the *c*-glide symmetry, that is a symmetry element for the host lattice, is absent. This is the reason for the appearance of the forbidden reflections mentioned above. Such a periodicity is not well defined but the faulted slabs are mixtures of the two types of *A* and *B* (indicated by *C*) and also the slabs are not planar. It is a reasonable assumption therefore that the defect *A* is a transitional form to the defect *B*. These faulted slabs may not be accompanied by an appreciable strain field but are coherently intergrown in the matrix. Similar types of faults have been commonly observed in 'block structures' and called 'Wadsley' defects.

The faulted slab *B* contains the tetrahedrally coordinated Nb atoms (indicated by circles) in positions which appear as dark spots in the image. We found that there is evidently some structural relationship between the faulted slab *B* and the superstructure described before. The locations of the periodic arrays of the tetrahedral positions are nicely in coincidence with those of the linear chains of the point-defect complexes in the superstructure (see hatched squares in Fig. 5). This implies that the defect slabs are created from reorganization of only some of the linear chains of the point-defect complexes (indicated by unhatched squares in Fig. 5) in the superstructure. The rearrangement of the blocks, *i.e.* the rearrangement of the CS planes, may be induced by dissipation of the point defects resulting from release of oxygen atoms from the crystal. The defects slabs discussed so far are observed in a matrix of ortho-$Nb_{12}O_{29}$.

On the other hand, if the matrix is monoclinic, the faulted slabs develop parallel to (102) [Fig. 7(*b*)]. There are also two types of contrast for the faulted slabs (marked *D* and *E*). They are considered to be essentially the same as the ones developed in the ortho-$Nb_{12}O_{29}$ in Fig. 7(*a*) and can be explained in the similar way. A possible model for the defect slab *E* is shown in Fig. 8(*b*). We did not observe the superstructure in the mono-$Nb_{12}O_{29}$ which was described as 'Ox-I' by Schäfer, Gruehn & Schulte (1966) and Browne, Hutchison & Anderson (1972), but there is no doubt that its structure also consists of a regular arrangement of the linear chains of the pairs of the point defects similar to the superstructure of ortho-$Nb_{12}O_{29}$ mentioned before.

An interesting thing in Fig. 7(*b*) is that near the terminations of the defects *E* the 3×5 blocks are formed (indicated by arrows). The examination of the termination of the faulted slabs and the displacements of the blocks may provide some information on the diffusion mechanism of the metal and oxygen atoms in the 'block structures' involved in transformations. The mechanism of the rearrangement of the blocks will be considered in a subsequent paper (Iijima, 1975*b*).

Finally it should be mentioned that all these faulted slabs disappear with further prolonged electron-beam irradiation and an ordered structure of $Nb_{12}O_{29}$ appears. Final images are very much the same as the one observed from the stoichiometric materials of $Ti_2Nb_{10}O_{29}$ which is isostructural with $Nb_{12}O_{29}$ (Iijima, 1971; Wadsley, 1961). Thus, it is certain that the crystals have been nearly completely reduced under the electron-beam irradiation. Since there was no change in the shape of the crystal after the reduction, crystal growth did not occur on the surface, which argues against the long migration of the cations. Therefore, all the structural changes described here involve a long migration of the oxygen atoms only.

It is of interest to examine how many extra oxygen atoms are involved in the formation of the faulted slabs with respect to the matrix structure. Let us consider the metal–oxygen ratio, for instance, in the faulted slabs *B* in Fig. 7(*a*). Although, as we will mention later, the true structure of the tetrahedral position is not fully understood, we assume that it has the ideal structure given by X-ray analysis. The result showed that the numbers of oxygen atoms and Nb atoms in the enclosed area in Fig. 8(*a*) are 154 and 64 respectively. When this region changes into the matrix structure, those numbers are 152 and 64, *i.e.*, in the formation of the faulted slabs there is no change in the number of the cations as we expected but an increase in the number of oxygen atoms. Here we assumed that a string of metal–oxygen –M–O– is inserted at the doubled tunnels indicated by $\times$'s in Fig. 8(*a*). From this we can confirm that the faulted slabs have an excess of oxygen and the metal–oxygen ratio in the slabs (O/M = 2·4375) becomes smaller than that of the superstructure. In other words the faulted slabs *B* may be formed during the reduction process of the superstructure.

Discussion

Short-range order

We have described the long-range ordering of the linear chains of point defects which takes place as a result of the aggregation of the point defects. It is interesting to notice that the positions for the pair of point defects in the superstructure are the nearest neighbors among the possible sites for point-defect complexes in the structure of ortho-$Nb_{12}O_{29}$. This fact implies that a pair of point defects may be more stable than an isolated one, perhaps because a symmetric arrangement of the atoms in the defect regions will be favored energetically over the asymmetrical one. A large separation (about 12 Å) between the paired defects suggests that the interaction force between them is elastic rather than Coulombic. The distortion around the pair of the defects will be relaxed over a large distance and the strain field around the defects may be interacting with those of the neighboring defect pairs, resulting in a long-range interaction between individual defects. The long-range forces are minimized for an arrangement of defect pairs and, as a result, the superstructure will be formed. This is a general concept for the formation of superstructures.

Then the question arises as to whether point-defect complexes have already occurred in pairs in the original crystals of $Nb_{12}O_{29}$ with an excess content of oxygen and formed short-range order. However, no indication of short-range order appeared in the electron micrographs, probably because they only show a two-dimensional projection of the structure along the incident electron beam, but the electron diffraction pattern showed the diffused bands in Fig. 2(*a*). Here we shall interpret the diffuse bands and consider the possibility of the occurrence of short-range order of the point defects.

The structure of the pair of point defects (Fig. 4) is created by slight displacements of the cations and oxygens as well as some interstitial oxygens, and the point defects form a chain of limited length along [010]. The percentage of displaced metal atoms compared to those of the matrix structure is 5·6%. Thus, the matrix structure and the superstructure may not differ appreciably in their electron diffraction patterns, and the main contributions to the superstructure spots may come from the distortions of the matrix structure itself, which are induced by the chains of the point defects. The distortion in the matrix will be generated in such a way that the chains attract each other because they tend to form pairs. By considering the symmetry in the distribution of the defect pairs (Fig. 5), we can expect that displacements of the atoms occur along [001] toward the lines parallel to [100] (indicated by thick horizontal arrows) where the chains of point defects occur twice as densely as in the others (thin arrows). The shift of the groups of atoms is schematically illustrated on the left-hand side of Fig. 5 (see the displaced peaks drawn with dotted lines).

Interpretation of the diffraction patterns from distorted crystals is given in various publications (for instance, Cowley, 1975). Let us consider the Patterson method for this problem. Generally a distorted crystal can be expressed by $\varrho(\mathbf{r}) = \bar{\varrho}(\mathbf{r}) + \Delta\varrho(\mathbf{r})$, where $\varrho(\mathbf{r})$ is the actual charge distribution in a distorted crystal, $\bar{\varrho}(\mathbf{r})$ is an averaged charge distribution and represents a periodic lattice, $\Delta\varrho(\mathbf{r})$ is a deviation from the averaged lattice. Then the Patterson function is

$$P(\mathbf{r}) = \bar{\varrho}(\mathbf{r}) * \bar{\varrho}(-\mathbf{r}) + \Delta\varrho(\mathbf{r}) * \Delta\varrho(-\mathbf{r})$$

or,

$$|F(\mathbf{u})|^2 = |\bar{F}(\mathbf{u})|^2 + |\Delta F(\mathbf{u})|^2.$$

The observed intensity $|F(\mathbf{u})|^2$ is separated into two parts, *i.e.* sharp Bragg reflections from the averaged lattice $|F(\mathbf{u})|^2$ and diffuse scattering $|\Delta F(\mathbf{u})|^2$ in the background. If $\Delta\varrho(\mathbf{r})$ is partly periodic over some regions owing to short-range order, the intensities of the diffuse scattering will be modulated.

Now, for the present case, consider a Fourier component of F_{00l}. We take $\varrho_0(\mathbf{z})$ for the charge distribution projected onto (100) of the matrix structure as shown in Fig. 5. $\varrho_0(\mathbf{z})$ is a periodic array with a period $c/2$. At both sides of the peaks $\varrho_0(\mathbf{z})$ is indicated by thick arrows, $\varrho_0(\mathbf{z})$ are assumed to be displaced by $\pm\Delta$, which is indicated by dotted lines.
Then, we obtain

$$\varrho(\mathbf{z}) = \varrho_0(\mathbf{z})*\delta(\mathbf{z}) + \varrho_0*\delta(\mathbf{z}-C/2+\Delta) + \varrho_0(\mathbf{z})*\delta(\mathbf{z}+C/2-\Delta)$$

$$\bar{\varrho}(\mathbf{z}) = \varrho_0(\mathbf{z})*\delta(\mathbf{z}) + \varrho_0(\mathbf{z})*\delta(\mathbf{z}-C/2) + \varrho_0(\mathbf{z})*\delta(\mathbf{z}+C/2)$$

$$\Delta\varrho(\mathbf{z}) = \varrho_0(\mathbf{z})*\{\delta(\mathbf{z}-C/2+\Delta)-\delta(\mathbf{z}-C/2)\} + \varrho_0(\mathbf{z})*\{\delta(\mathbf{z}+C/2-\Delta)-\delta(\mathbf{z}+C/2)\},$$

where $\delta(\mathbf{z})$ is a delta function around which $\varrho_0(\mathbf{z})$ is centered, and $*$ represents the convolution operation.

Then we have the defect Patterson function

$$\mathscr{F}[\Delta\varrho(\mathbf{z})*\Delta\varrho(-\mathbf{z}) = |\Delta F(\mathbf{w})|^2 = 4f_{\mathrm{O}}\sin^2\pi\mathbf{w}(C-\Delta)\sin^2\pi\mathbf{w}\Delta .$$

The last equation tells us that the diffuse background due to the lattice distortion is modulated by a period of $\frac{1}{2}c$ corresponding to d_{002} of the ortho-$Nb_{12}O_{29}$ and the intensities of the diffuse scattering become nearly zero near the positions of the sharp reflections from the averaged lattice since the displacement vector Δ is very small compared with $\mathbf{c}/2$. Also the intensity maxima of the diffuse scattering increase with the distance from the origin. This crude consideration explains qualitatively the observation of the diffuse scattering of Fig. 2(*a*). The continuous diffuse bands along [100] indicate that the defect pairs which are extended to [010] tend to order only along [001], forming slabs parallel to the (100) plane (the positions of the slabs are indicated by vertical arrows in Fig. 5) and each slab may form almost independently of the neighboring slabs.

As we mentioned previously, the point defects also tend to order along [010]. From these facts we may conclude that the point defects have been formed in a short-range ordered array in the original materials. It appears that the domains of the short-range order may grow with an intense electron-beam irradiation to form the superstructure.

Structure of the paired point defects

In the previous experiment (Iijima, Kimura & Goto, 1974), we found that the tetrahedral positions in crystals of $Nb_{22}O_{54}$ having nonstoichiometric compositions frequently showed considerable fluctuations in contrast and we thought that this could have been caused by some disorder in those positions, associated with an excess of oxygen. Anderson *et al.* (1973) studied the nonstoichiometry of $GeNb_{18}O_{47}$ and suggested that there are some interstitial metal atoms in the column of the tetrahedral positions [shaded area in Fig. 4(*d*)] and similar defects may occur widely in the Nb oxides having an oxygen deficiency. The elucidation of these problems is important for understanding the nonstoichiometric properties of the Nb oxides.

One of the clues for this question may be obtained by considering the structure of the paired point-defect complexes since the similarity between the contrasts at the tetrahedral positions and the point defects is apparent. In the present experiment we found that the total number of the metal atoms in the regions showing the black spots in Fig. 3(*b*) is exactly the same as that of the matrix, so that dark contrast at the tetrahedral positions results from only small displacements of the metal atoms from the original sites in the matrix. In other words the dark contrast at the tetrahedral positions does not involve an increase in the number of the metal atoms. Furthermore the paired point defects tend to order along [010] with a period of $2b$.

Keeping this in mind, we suggest tentatively a model for the linear chains of the paired point-defect complexes in the superstructure which is slightly modified from that of Fig. 4(*a*). An *ac* plane projection of the defects is illustrated in Fig. 4(*e*) which corresponds to the shaded area of Fig. 4(*a*). It is actually a superposition of the two structures shown in Figs. 4(*c*) and 4(*d*). These two structures might be alternated along [010], producing a doubling of the *b* axis as observed in this experiment. Therefore in the projection [Fig. 4(*e*)] one half of the tetrahedrally coordinated atom positions (shown by small open circles) are occupied and the other half of the metal atoms are located evenly at either of two octahedral sites (indicated by solid circles). However the displaced metal atoms (indicated by A and B) also may have possibilities of going to the sites indicated by × 's. In this model, the location of the interstitials of the oxygen atoms is not clear, but they should exist in the column of tetrahedral positions because occurrence of such tetrahedral positions in $Nb_{12}O_{29}$ contributes to the excess content of the oxygen.

One means of justifying this model will be obtained by finding an adequate interpretation of the image contrast of the lattice images. The calculation of the two-dimensional lattice images for the high-resolution micrographs has been well established (Fejes, 1973) and the calculated images show a good agreement with the experimental images. The recent calculation of the image contrast for the tetrahedral positions by Skarnulis, Iijima & Cowley (1975) raises a question as to whether the dark contrast cannot be produced at the tetrahedral positions by using the structure originally given by X-ray diffraction analysis. Atoms in the ideal tetrahedral positions always give a lighter contrast. A good agreement of the calculated images with the experiments, however, was obtained by assuming some

disorder of the atoms within a column parallel to [010] similar to the present model. Such disorder of atoms occurring along [010] has been proposed to explain the abnormal black contrast observed in the faulted crystals of H-Nb_2O_5 (Fig. 11 of Iijima, 1973). A similar argument, therefore, may hold for the explanation of the dark contrast of the linear chains of the paired point defects and the point-defect complexes cannot be described simply in terms of an ideal tetrahedrally coordinated metal atom.

The author wishes to thank Professor J. M. Cowley for his continuous encouragement and critical reading of the manuscript. This work was supported by NSF Grant (GH 36668).

References

ANDERSON, J. S., BROWNE, J. M., CHEETHAM, A. K., VON DREELE, R., HUTCHISON, J. L., LINCOLN, F. J., BEVAN, D. J. M. & STRAEHLE, J. (1973). *Nature, Lond.* **243**, 81–83.

BROWNE, J. M., HUTCHISON, J. L. & ANDERSON, J. S. (1972). *Proc. of 7th Int. Symp. on Reactivity of Solids., Bristol*, pp. 116–124.

COWLEY, J. M. (1975). *Diffraction Physics*. Amsterdam: North-Holland.

FEJES, P. L., IIJIMA, S. & COWLEY, J. M. (1973). *Acta Cryst.* A**29**, 710–714.

FEJES, P. L. (1973). Ph. D. Thesis, Arizona State Univ.

IIJIMA, S. (1971). *J. Appl. Phys.* **42**, 5891–5893.

IIJIMA, S. (1973). *Acta Cryst.* A**29**, 18–24.

IIJIMA, S. (1975*a*). *J. Solid State Chem.* **14**, 52–65.

IIJIMA, S. (1975*b*). In preparation.

IIJIMA, S. & ALLPRESS, J. G. (1973). *J. Solid State Chem.* **7**, 94–105.

IIJIMA, S., KIMURA, S. & GOTO, M. (1974). *Acta Cryst.* A**30**, 251-257.

IIJIMA, S., KIMURA, S. & GOTO, M. (1973). *Acta Cryst.* A**29**, 632–636.

KIMURA, S. (1973). *J. Solid State Chem.* **6**, 438–449.

SCHÄFER, H., GRUEHN, R. & SCHULTE, F. (1966). *Angew. Chem.* **5**, 28–41.

SKARNULIS, A. D., IIJIMA, S. & COWLEY, J. M. (1975). To be published.

WADSLEY, A. D. (1961). *Acta Cryst.* **14**, 664–670.

Acta Cryst. (1975). A**31**, 790

Dérivation par Induction de Groupes d'Espace et de Groupes Magnétiques

PAR JEAN SIVARDIÈRE

Département de Recherche Fondamentale, Laboratoire de Chimie Physique Nucléaire, Centre d'Etudes Nucléaires de Grenoble, B.P. 85 – 38041 *Grenoble Cedex, France*

(*Reçu le* 25 *septembre* 1974, *accepté le* 22 *mai* 1975)

Starting from space groups, the point groups of which are cyclic, all the other space groups are deduced. The inductive method used is known to provide the 32 point groups, starting with the cyclic groups. It is applied to the derivation of magnetic point and space groups.

I. Introduction

Une méthode classique d'énumération des groupes d'espace est celle de Zachariasen (1951): elle fournit tous les groupes d'espace G_e de classe G et de réseau T donnés en exploitant les relations entre éléments générateurs de G. Elle permet aussi bien d'énumérer les groupes d'espace magnétiques (Sivardière, 1970). Une méthode voisine d'énumération (Sivardière & Bertaut, 1970) utilise également la structure d'extension des groupes d'espace: G_e est une extension de $G \times G$ par le groupe T des translations du réseau. Il est enfin possible d'utiliser une propriété d'additivité des groupes d'espace (Sivardière, 1969). La méthode d'énumération proposée dans cet article n'utilise pas la structure d'extension des groupes d'espace: partant d'un groupe d'espace H_e quelconque, nous recherchons directement les éléments $(\alpha|\tau_\alpha)$ qui, avec les éléments de H_e, engendrent un sur-groupe G_e; ces éléments doivent réaliser un automorphisme externe de H_e; H_e est un sous-groupe invariant maximal de G_e.

Cette méthode inductive permet de construire les 32 groupes ponctuels à partir des groupes cycliques propres ou impropres (Lomont, 1959; Sivardière & Bertaut, 1970). Elle met en évidence la structure algébrique (produit direct ou semi-direct) des groupes ponctuels et se généralise à l'étude des groupes ponctuels magnétiques. Ainsi, partons du groupe $H=4$; un axe 2_x perpendiculaire à l'axe 4_z réalise des automorphismes externes des éléments du groupe H puisque:

$$2_x(4_z) = 2_x 4_z 2_x^{-1} = 4_z^3 .$$

D'où le groupe produit semi-direct:

$$G = 422 = 4_A 2 .$$